COMMUNICATIONS IN NUMERICAL METHODS IN ENGINEERING
Commun. Numer. Meth. Engng (in press)
Published online in Wiley InterScience (www.interscience.wiley.com). DOI: 10.1002/cnm.908

On the resolution of transverse stresses in solid-shells with a multi-layer formulation

M. Fiolka and A. Matzenmiller*, †

Institute of Mechanics, University Kassel, Germany

SUMMARY

A locking free solid-shell element, based on a surface orientated shell formulation, is used for a single-layer approach as well as for a multi-layer analysis. Locking is removed by a combination of the assumed strain and enhanced assumed strain methods. The suggested incompatible strain field enables the element to pass the patchtest for plates with a minimum of enhancement parameters. It is tested at various benchmark examples for the resolution of the transverse shear and normal stresses in thin-walled structures. Copyright © 2006 John Wiley & Sons, Ltd.

Received 18 October 2005; Revised 17 March 2006; Accepted 26 June 2006

KEY WORDS: transverse shear and normal stress; solid-shell element; multi-layer formulation; locking phenomena in shells; EAS method; patchtest; benchmark examples; curved beam; condition number

1. INTRODUCTION

A three-dimensional theory for thin-walled structures is advisable for the precise modelling of shells at the bearings and in the contact zone, where concentrated loads are applied, as well as for the abrupt transition from thick to thin structural members. If both shell embrasures are used for the explicit description of the position vector of any point in the shell body, the outcome is the surface orientated shell formulation [1, 2] with complete stress and strain tensors, allowing the incorporation of non-degenerated three-dimensional material models. The incompatible strain field, enhanced with three parameters, enables the element to pass the patchtest. However, a multi-layer formulation (MLF) [3] is necessary for the complete resolution of the three-dimensional state of deformation and stress. The MLF comprises the representation of the transverse normal stresses, caused by loadings normal to the shell surface or encountered in curved shell structures under

*Correspondence to: A. Matzenmiller, Institute of Mechanics, University Kassel, 34109 Kassel, Mönchebergstr. 7, Germany.
†E-mail: post-structure@uni-kassel.de

bending. The multi-layer approach used here is immediately applicable to the analysis of laminated shell structures.

2. SHELL KINEMATICS

The position vector $\mathbf{X}$ of a material point $\mathscr{P}$ of the shell body is described by the position vector of points on the upper and lower shell embrasure $\mathbf{X}^{\mathrm{u}}$ and $\mathbf{X}^{\mathrm{l}}$ and a normalized parameter θ in thickness direction ($-1 \leqslant \theta \leqslant 1$), see Figure 1.

$$\mathbf{X}(\boldsymbol{\xi}) = \tfrac{1}{2}[(1+\theta)\mathbf{X}^{\mathrm{u}}(\xi,\eta) + (1-\theta)\mathbf{X}^{\mathrm{l}}(\xi,\eta)] \quad \text{with } \boldsymbol{\xi} = (\xi,\eta,\theta) \tag{1}$$

This kinematical assumption ensures that material lines between the embrasures remain straight during the deformation according to the Bernoulli-hypothesis. As it is typical in shell modelling a midsurface with the position vector $\mathbf{X}^m$

$$\mathbf{X}^m(\xi,\eta) = \tfrac{1}{2}[\mathbf{X}^{\mathrm{u}}(\xi,\eta) + \mathbf{X}^{\mathrm{l}}(\xi,\eta)] \tag{2}$$

is introduced in Equation (1), rewritten as

$$\mathbf{X}(\boldsymbol{\xi}) = \tfrac{1}{2}[\mathbf{X}^{\mathrm{u}}(\xi,\eta) + \mathbf{X}^{\mathrm{l}}(\xi,\eta)] + \tfrac{1}{2}\theta[\mathbf{X}^{\mathrm{u}}(\xi,\eta) - \mathbf{X}^{\mathrm{l}}(\xi,\eta)] \tag{3}$$

It leads to

$$\mathbf{X}(\boldsymbol{\xi}) = \mathbf{X}^m(\xi,\eta) + \tfrac{1}{2}\theta H(\xi,\eta)\mathbf{D}(\xi,\eta) \tag{4}$$

with the shell director

$$\mathbf{D}(\xi,\eta) = \frac{\mathbf{X}^{\mathrm{u}}(\xi,\eta) - \mathbf{X}^{\mathrm{l}}(\xi,\eta)}{\|\mathbf{X}^{\mathrm{u}}(\xi,\eta) - \mathbf{X}^{\mathrm{l}}(\xi,\eta)\|} \tag{5}$$

The shell director $\mathbf{D}$ is a unit vector, which describes the rotation of the cross sections during the motion of the shell body. The shell thickness H may change during the deformation process.

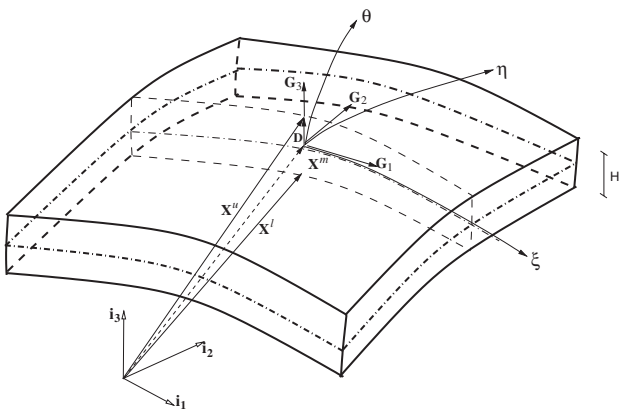

Figure 1. Solid-shell.

DOI: 10.1002/cnm

The shell has six kinematical degrees of freedom, which are the three displacement components of the upper and lower points of the cross section. Hence, the mechanical formulation is called a 6-parameter shell theory.

3. STRATEGIES AGAINST LOCKING

Enhanced solid elements with eight nodes and trilinear shape-functions are applied for the discretization of thin-walled bodies. The solid elements used are locking free and show a similar convergence performance as shell elements do. Convective co-ordinates are used for the description of stress and strain tensors of the shell body. The standard linear solid element shows the well-known locking effects as a consequence of the low-order interpolation for the displacement field. The locking phenomena can be avoided by means of a combination of the assumed strain (AS) and enhanced assumed strain (EAS) method.

3.1. Shear locking

Low-order interpolated elements are unable to represent pure bending deformations exactly. Bending deformations are dominated by spurious shear deformations. The AS method, developed by Bathe and Dvorkin [4], circumvents shear locking in states of pure bending.

3.2. Thickness or curvature locking

Artificial thickness strains arise in coarse meshes with linear elements of initially curved structures or geometrically non-linear analysis even in states of pure bending with a vanishing Poisson's ratio. This leads in coarse finite element meshes to overstiff element behaviour, called thickness locking, first noticed by Verhoeven [5]. It can be cured by the AS method. Similar remedies for solid-shell elements with an extensible director are proposed in References [6, 7] and successfully applied.

3.3. Transverse straining

In order to use non-degenerated, complete three-dimensional constitutive models together with the single-layer formulation (SLF), the shell approach must accept the complete tensors for the stress and strain state including the linear variation of the transverse normal strain E_{33}, occurring in all states of bending, if Poisson's ratio ν is unequal to zero. By means of the EAS method [8], based on the Hu–Washizu functional, the linear part for the distribution of thickness strains may be provided by an incompatible strain field. As a consequence of this additional degree of freedom a 7-parameter theory [9] comes into being. The incompatible strain field of the Green–Lagrange type $\tilde{\mathbf{E}}$ is introduced successfully with a contravariant basis $\mathbf{G}_0^i$ at the element centre in order to meet the necessary requirements of the EAS method—see Reference [8].

$$\tilde{E}_{ij}\mathbf{G}^i \otimes \mathbf{G}^j = \tilde{E}^0_{kl}\mathbf{G}^k_0 \otimes \mathbf{G}^l_0 \;\Leftrightarrow\; \tilde{E}_{ij} = \mathbf{G}_i \cdot \mathbf{G}^k_0 \tilde{E}^0_{kl}\mathbf{G}^l_0 \cdot \mathbf{G}_j \tag{6}$$

with the covariant base vectors given as

$$\mathbf{G}_1 = \frac{\partial \mathbf{X}}{\partial \xi}, \quad \mathbf{G}_2 = \frac{\partial \mathbf{X}}{\partial \eta}, \quad \mathbf{G}_3 = \frac{\partial \mathbf{X}}{\partial \theta}$$

DOI: 10.1002/cnm

and the contravariant ones of the element centre $\xi = \eta = \theta = 0$:

$$\mathbf{G}_0^1 = \frac{\partial \xi}{\partial \mathbf{X}}, \quad \mathbf{G}_0^2 = \frac{\partial \eta}{\partial \mathbf{X}}, \quad \mathbf{G}_0^3 = \frac{\partial \theta}{\partial \mathbf{X}}$$

The matrix $\mathbf{T}^0$ [10] is introduced to transform between the basis systems at the element centre and the contravariant basis system at the Gauss-points on the initial configuration of each element as defined in Equation (6):

$$\tilde{\mathbf{E}} = \mathbf{T}^0 \tilde{\mathbf{E}}^0 \quad \text{with } \tilde{\mathbf{E}}^0 = \frac{1}{\det \mathbf{J}} \mathbf{M} \alpha \tag{7}$$

where $\mathbf{M}$ is a matrix containing the monomials of the approximation for the spatial distribution of incompatible thickness strains and $\boldsymbol{\alpha}$ comprises the free strain parameters:

$$\boldsymbol{\alpha} = \begin{bmatrix} \alpha_1 \\ \alpha_2 \\ \vdots \end{bmatrix}$$

The enhancement of the constant thickness strain may already be achieved by one parameter α_1 and

$$\mathbf{M} = \begin{bmatrix} 0 \\ 0 \\ \theta \\ 0 \\ 0 \\ 0 \end{bmatrix} \tag{8}$$

only linear in normal direction, or by a complete linear extension of thickness strains E_{33} in θ-direction with three parameters α_1 to α_3 and

$$\mathbf{M} = \begin{bmatrix} 0 & 0 & 0 \\ 0 & 0 & 0 \\ \theta & \theta\xi & \theta\eta \\ 0 & 0 & 0 \\ 0 & 0 & 0 \\ 0 & 0 & 0 \end{bmatrix} \tag{9}$$

4. MULTI-LAYER FORMULATION

The MLF assumes a piecewise linear course of the material lines in thickness direction of the deformed shell [7] whereby the Bernoulli-hypothesis is abandoned. The shell body is subdivided

DOI: 10.1002/cnm

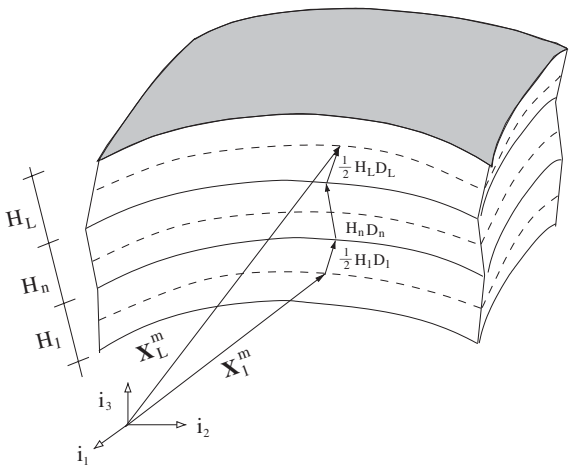

Figure 2. Multi-layer kinematics.

into layers of finite thickness with a director at every layer midsurface. An arbitrary material point at the midsurface of layer L of the shell can be identified by the position vector of the first layer $\mathbf{X}_1^m$ and a sum of layer directors $\sum H_n \mathbf{D}_n$—see Figure 2.

$$\mathbf{X}_L^m(\xi,\eta) = \mathbf{X}_1^m(\xi,\eta) + \frac{1}{2}H_1(\xi,\eta)\mathbf{D}_1(\xi,\eta) + \sum_{n=2}^{L-1} H_n(\xi,\eta)\mathbf{D}_n + \frac{1}{2}H_L(\xi,\eta)\mathbf{D}_L(\xi,\eta) \tag{10}$$

This MLF approximates every transverse stress distribution for the shear and normal component through the thickness by a step function. Consequently, a shear correction factor for an insufficient transverse shear stress distribution is not necessary in the multi-layer model. The correct distribution of the normal stress component in thickness direction, caused by loading normal to the shell surface, can be approximated by a constant course within each layer of the model.

5. NUMERICAL EXAMPLES

Five numerical examples are presented to verify the shell formulation and demonstrate its performance. The standard eight node solid element is denoted as ssh8 in the following graphs. The letters A and E are added to this abbreviation for the solid-shell element when the AS method, discussed in Chapters 3.1 and 3.2 or the EAS method discussed in Chapter 3.3 are applied. For the latter case the number of enhancement parameters, 1 or 3, is added to the denotation in accordance with the spatial distributions as given in Equations (8) and (9). The results of the analysis with the solid-shell element, proposed above in context with the SLF, are compared to the ones obtained with the 5-parameter theory of four node shell elements for the discretization of the shell reference surface. The 5-parameter shell element, denoted as sh4A, are based on the deformation of a shell reference surface with an inextensible director to describe the motion as given in References [11, 12]. There a degenerated constitutive tensor equation had to be used as a result of the assumption of the zero thickness stress and subsequent condensation of normal thickness

DOI: 10.1002/cnm

strains. In Reference [13] the normal thickness strains are included in the shell approach by means of the EAS extension, thus, allowing to incorporate complete three-dimensional material models. The elements are implemented into the program FEAP [14].

5.1. Patchtest

A necessary condition for the finite element method to produce convergent results as the element size decreases requires that an element passes the simple patch test as outlined in Reference [14, pp. 293–295]. The patchtest, published in Reference [15], for plate elements in the case of constant bending is—i.e. a homogeneous state of bending throughout a path of elements—applied to check, whether the solid-shell element is able to represent rigid body motions and homogeneous distributions of bending and twisting moments exactly. In order to test shell elements, a parabolic displacement field $w(x, y)$ as given in Equation (11), and two rotations $b_x(x, y)$, $b_y(x, y)$—see Equations (12) and (13)—are applied to the four edges of a rectangular patch, consisting of five arbitrarily shaped elements—see Figure 3. The shell element passes the patchtest, if the displacements of the interior nodes 1 to 4 from the FE-analysis satisfy the analytically computed displacement $w(x, y)$ and rotation $b_x(x, y)$, $b_y(x, y)$ fields exactly. The deformation of the reference surface ($\theta = 0$) may be computed from the position vector in small displacement theory according to:

$$w(x, y) = 0.5 \times 10^{-3}(x^2 + xy + y^2) \tag{11}$$

$$b_x(x, y) = \frac{\partial w}{\partial y} = 10^{-3}(y + x/2) \tag{12}$$

$$b_y(x, y) = -\frac{\partial w}{\partial x} = 10^{-3}(-x - y/2) \tag{13}$$

The second derivatives of $w(x, y)$ are all constant and thus, generate a state of homogeneous bending. Since the solid-shell element has no rotational degrees of freedom, but nodal points out of the reference plane, the three components of the displacement vector at the nodes on the upper and lower surface, indexed by u and l, are computed from:

$$[u, v, w]_{\mathrm{u}}^{\mathrm{l}} = \left[\mp \frac{h}{2} b_y, \pm \frac{h}{2} b_x, w\right] \tag{14}$$

with the thickness $h = 0.001$. Table I shows the calculated displacements of nodes 1 to 4 for the elements ssh8AE1 and ssh8E3 for the case of a single layer of elements (SLF). The ssh8AE3

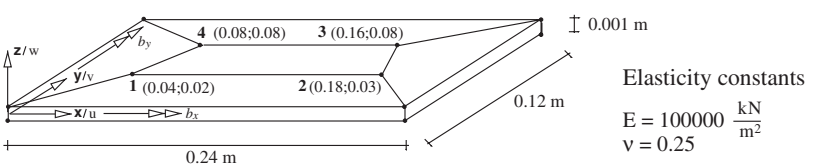

Figure 3. Patchtest with five elements, nodal co-ordinates and positve rotations b_x and b_y about x- and y-axis.

DOI: 10.1002/cnm

Table I. Displacements (m) of node 1 to 4 for one (ssh8AE1) and three (ssh8AE3) parameters.

ssh8AE1	$-u \times 10^{-8}$	$-v \times 10^{-8}$	$w \times 10^{-6}$
(a) *one* (*ssh8AE1*)			
1	2.494	2.002	1.398
2	9.749	5.943	19.33
3	10.05	8.011	22.34
4	5.934	5.976	9.556
ssh8AE3	$-u \times 10^{-8}$	$-v \times 10^{-8}$	$w \times 10^{-6}$
(b) *three* (*ssh8AE3*)			
1	2.500	2.000	1.400
2	9.750	6.000	19.35
3	10.00	8.000	22.40
4	6.000	6.000	9.600

element passes the patch test as the results in Table I(b) correspond to the exact displacement values from Equations (11) to (13), evaluated with the co-ordinates of nodes 1 to 4. However, if the thickness strains are enhanced only with one parameter, as it is the case for element ssh8AE1, the patchtest is failed—see Table I(a) and Reference [16]. Thus, it is essential to enhance the thickness strains at least by a complete linear extension of the thickness co-ordinate with three parameters, as given by Equation (9), so that the element passes the patchtest, as the results in Table I(b) prove.

5.2. Pinched hemisphere—comparison of SLF with 5-parameter shell theory

The double curved shell in Reference [17] serves as an example to show that the present solid-shell element can produce results as good as the 5-parameter theory for moderately thin plates. The hemispherical shell has a radius of 10 mm and is 0.5 mm thick. The elasticity modulus is equal to $10\,\mathrm{N/mm^2}$ and Poisson's ratio is equal to 0.2. The structure is loaded by two orthogonal unit forces F—see Figure 4(a). Due to symmetry only one quarter of the shell is modelled. The finite element mesh is composed by three patches of each with 64 elements. The analysis type is geometrically non-linear, since the deformations are large—see Figure 4(b). The final load is applied in five loadsteps, until the loadfactor of 0.05 N is reached. The standard solid element ssh8 without any enhancements shows a stiffer behaviour in comparison to the shell elements sh4A in Reference [12] and sh4AE8 in Reference [13]—see Figure 4(b). With the enhancement by the EAS and AS method the locking effects can be eliminated and the two shell elements sh4A and sh4AE8 lead to the same results as the solid shell element ssh8AE3 does—see solid line in Figure 4(b). Figure 5 shows the computation time for a mesh with 4, 16, 64 and 256 elements per patch. The enhanced solid-shell ssh8AE3 needs only about 10% more computation time than the standard solid element ssh8. About three times as much computation time is needed for the solid-shell element in comparison to the shell element for a patch with 256 elements. However, this additional computational expense is due to the fact that twice as many nodal points and thus about 20% more degrees of freedom occur in the solid-shell formulation in comparison to the shell approach. Most of the extra numerical operations are needed for the decomposition of the larger stiffness matrix.

DOI: 10.1002/cnm

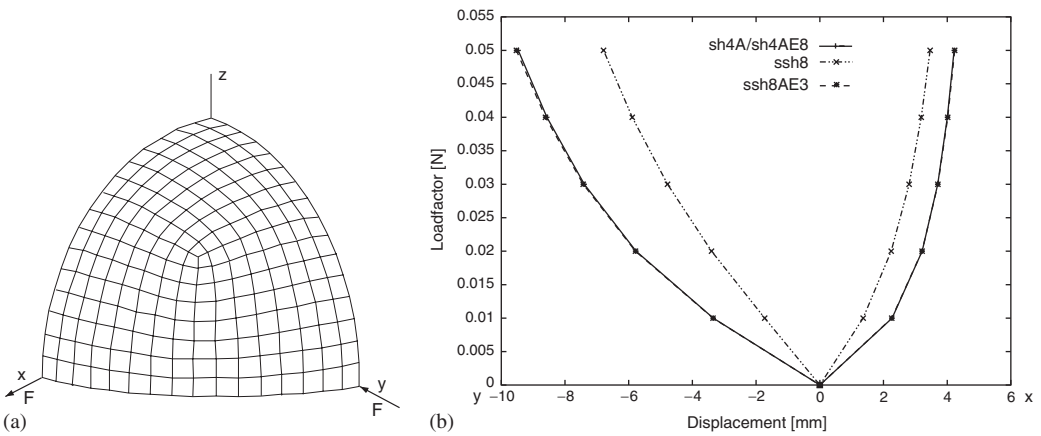

Figure 4. (a) Quarter model of the pinched hemisphere; and (b) displacement diagram on the x- and y-axis.

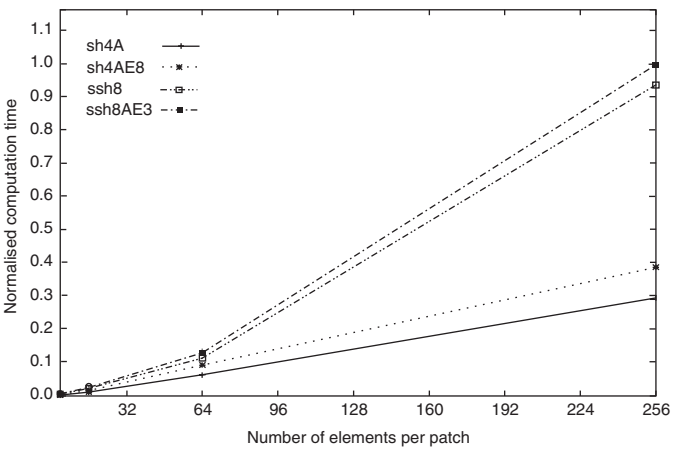

Figure 5. Computation time normalized with respect to largest runtime versus number of elements per patch.

5.3. Cantilever beam

The cantilever beam of Figure 6 is modelled with 10 elements in length direction, one element over the width and a variable number of kinematic layers through the height (MLF). All degrees of freedom are suppressed at the bearing point. With a rising number of layers the shell element approximates the analytical solution of engineering mechanics for the thickness stress σ_{33}:

$$\sigma_{33} = -\frac{q}{2} + q\left[\frac{1}{4}\left(\frac{z}{h}\right)^3 - \frac{3z}{4h}\right] \tag{15}$$

DOI: 10.1002/cnm

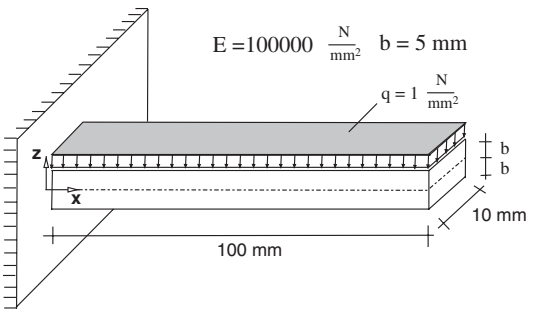

Figure 6. Cantilever beam.

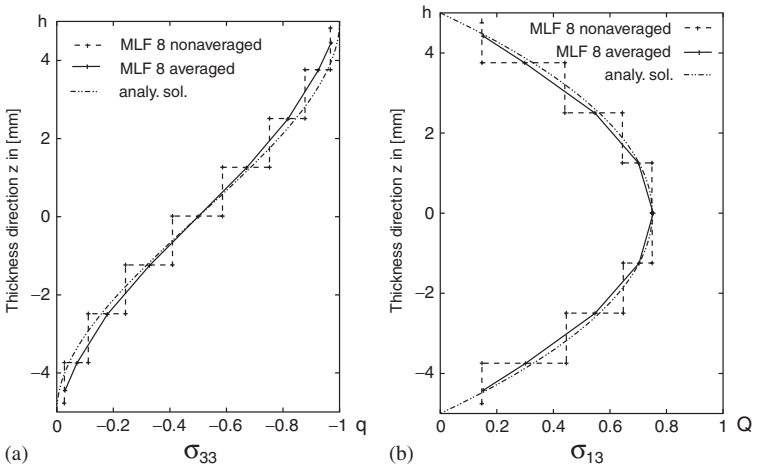

Figure 7. (a) Distribution of thickness stress; and (b) transverse shear stress over cross section for $v = 0.0$ and 8 layers.

and for the transverse shear stress σ_{13}:

$$\sigma_{13} = \frac{3Q}{4b}\left[1 - \left(\frac{z}{h}\right)^2\right] \tag{16}$$

more closely. Figure 7 shows the transverse stresses, obtained as a discontinuous step function form a mesh with eight layers of solid-shell elements from the 6- and 7-parameter theory. The results are given at the cross-section in the midsection of the cantilever beam, in order to exclude boundary influences at the tip and at the clamped edge as far as possible. The transverse stresses are computed with Poisson's ratio equal to $v = 0.0$ in order to compare them with the analytical solution, given for vanishing Poisson ratio only. The averaged values of the numerical results at the layer boundaries are added to the diagram as well as the analytical solution.

Figure 8 shows the displacement at the cantilever tip for the case of Poisson's ratio $v = 0.4$, plotted over the number of layers for the 6-parameter and the 7-parameter theory. The result

DOI: 10.1002/cnm

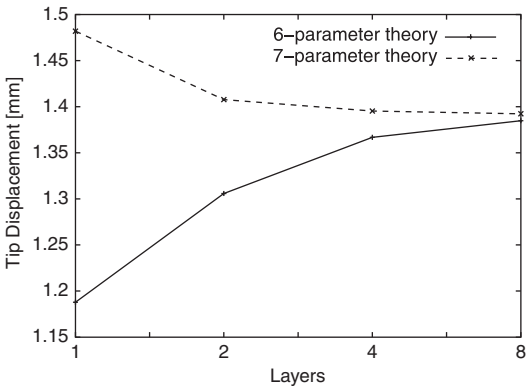

Figure 8. Displacement of midsurface at the tip of beam with $\nu = 0.4$.

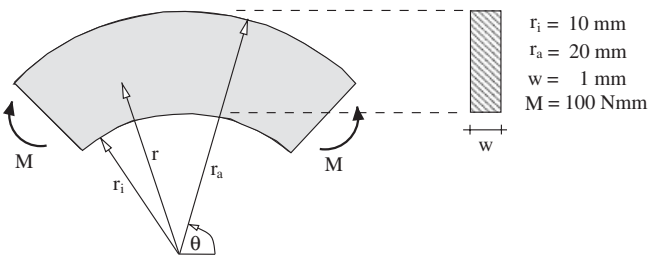

Figure 9. Curved bar under pure bending.

of the 6-parameter theory is to stiff, because of the non-existent linear thickness strain in the associated element—see Chapter 3.3. However the 6-parameter theory converges, but from below, i.e. from the 'stiffer side', while the 7-parameter theory converges from above ('soft side') towards the tip deflection of the complete, three-dimensional, converged solution. The difference of tip displacements between the SLF (one layer) and the MLF (eight layers) is computed for the 6-parameter theory to 14.5% and for the 7-parameter theory to 6.7%. The differences between the SLF and MLF are caused mainly by the insufficient approximation of the thickness stress distribution σ_{33}. The precise approximation of the shear stress σ_{13} is less important for the computation of the displacements. It should be noted that the transverse stress in the shell body under normal surface loading approximates the solution of the MLF theory as a constant distribution in each layer for both the 6-parameter (ssh8A) and 7-parameter (ssh8AE3) discretization—see Figure 7.

5.4. Curved bar

A 90°-sector of the curved bar is modelled in Figure 9 with 10 elements along the circumference and nine layers through the thickness. An approximate solution may be obtained from the

DOI: 10.1002/cnm

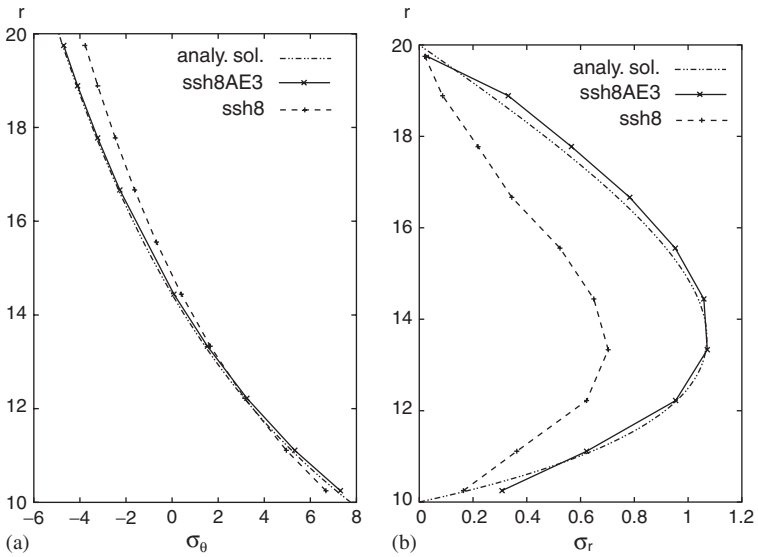

Figure 10. (a) Gradient of the circumferential stress; and (b) the radial stress averaged at the layer boundary.

hyperbolic bending theory of Winkler and Grashof [18]. Golovin developed an exact solution—see Reference [19, p. 71]. Equations (17) and (18) describe the circumferential stress σ_θ and the radial stress σ_r through the thickness as functions of the radius. The numerical results for the standard solid element ssh8 and the solid-shell element ssh8AE3 are compared to the analytical solution:

$$\sigma_\theta = -\frac{4M}{\mathrm{Det}}\left[-\frac{r_i^2 r_a^2}{r^2}\ln\frac{r_a}{r_i} + r_a^2\ln\frac{r}{r_a} + r_i^2\ln\frac{r_i}{r} + r_a^2 - r_i^2\right] \tag{17}$$

$$\sigma_r = -\frac{4M}{\mathrm{Det}}\left[\frac{r_i^2 r_a^2}{r^2}\ln\frac{r_a}{r_i} + r_a^2\ln\frac{r}{r_a} + r_i^2\ln\frac{r_i}{r}\right] \tag{18}$$

$$\mathrm{Det} = (r_a^2 - r_i^2)^2 - 4r_i^2 r_a^2\left(\ln\frac{r_a}{r_i}\right)^2 \tag{19}$$

The solid-shell element ssh8AE3 provides the distribution of circumferential stress very closely to the analytical solution—see Figure 10. Even the standard element ssh8 achieves an acceptable solution for the circumferential stress. The element ssh8AE3 approximates the radial stress distribution well, but the solution of the solid element ssh8 differs more than 40% from the analytical solution.

DOI: 10.1002/cnm

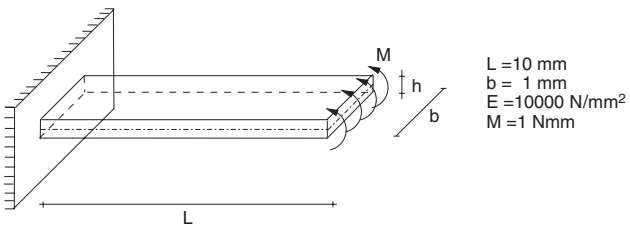

Figure 11. Cantilever beam under bending.

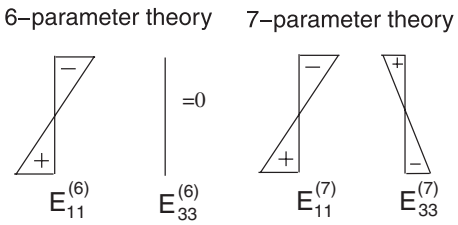

Figure 12. Transverse thickness strains.

5.5. *Pure bending*

Pure bending of finite element meshes is tested with a cantilever model, loaded by a moment at the tip—see Figure 11. The beam is modelled with 10 elements in length direction and one element over the width:

(i) *Transverse thickness strains*: If Poisson's ratio v is unequal to zero, the element from the 6-parameter theory (ssh8A) locks because of the non-existent linear thickness strain—see Chapter 3.3. For pure bending Braun [7] computed the order of the locking effect to $(E_{11}^{(7)} - E_{11}^{(6)})/E_{11}^{(7)} = v^2$—see also the result in Figure 8 for one layer (SLF). The EAS method cures the 6-parameter theory by means of introducing linear thickness strains into the FE-model—see Figure 12.

(ii) *Element behaviour at the thin plate limit*: The condition number $c^{(7)}$ of the element stiffness matrix increases with the power of $(l_c/h)^4$ in the 7-parameter theory [20], if the thickness h of the solid-shell element ssh8A with length l_c decreases.

$$c^{(7)} = \frac{\lambda_{\max}}{\lambda_{\min}} < \frac{EA_c/h}{EI/l_c^3} = \frac{El_c^2/h}{El_c h^3/12l_c^3} \propto \left(\frac{l_c}{h}\right)^4 \tag{20}$$

The condition number $c^{(5)}$ of the element stiffness matrix increases with the power of $(l_c/h)^2$ in the degenerated shell approach, if the thickness h of the shell element sh4A with length l_c decreases.

$$c^{(5)} = \frac{\lambda_{\max}}{\lambda_{\min}} < \frac{EA_c/l_c}{EI/l_c^3} = \frac{Ehl_c/l_c}{El_c h^3/12l_c^3} \propto \left(\frac{l_c}{h}\right)^2 \tag{21}$$

DOI: 10.1002/cnm

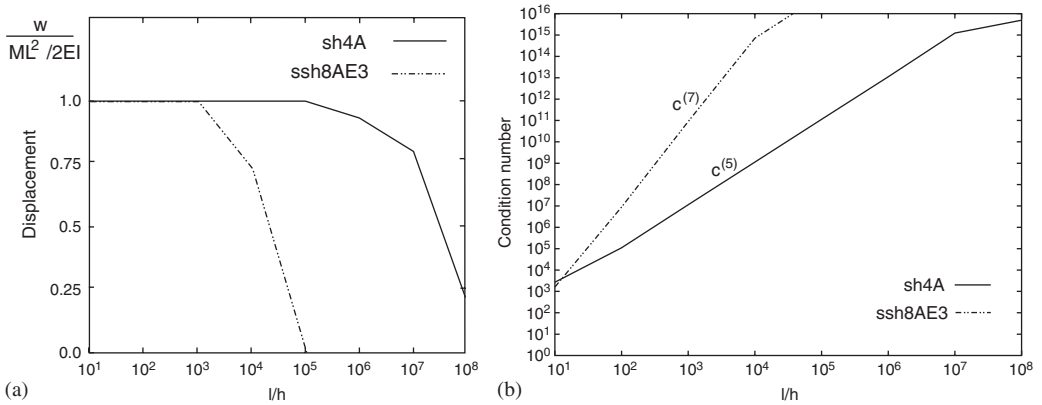

Figure 13. (a) Limit analysis with normalized displacement plotted versus the ratio of cantilever length l to thickness ratio h; and (b) condition number $c^{(5)}$ and $c^{(7)}$ plotted versus the ratio of length to thickness of cantilever.

In order to study the bending performance of the solid-shell element in the thin plate limit, the cantilever under a bending moment at the tip as shown in Figure 11, is investigated. The calculated tip deflection w is normalized with respect to $w/(Ml^2/2EI)$ and plotted versus the ratio of the cantilever length to the thickness h. As the thickness of the cantilever decreases, the FE result for the tip displacement deviates from the exact solution as $l/h > 10^3$ in the case of the solid-shell ssh8AE3, whereas the shell element sh4A diverges for $l/h > 10^5$—see Figure 13(a). The condition number of the structure stiffness matrix increases with the power of four for the solid-shell ssh8AE3 and with the power of two for the shell element sh4A—see Figure 13(b)—until the condition number exceeds the critical limit $>10^{14}$, where the system of equations becomes badly conditioned. Obviously, hardly any shell structure shows a length to thickness ratio of $l_c/h \gg 10^4$. However, the analysis of the cantilever is continued up to $l/h = 10^8$ in Figure 13(a) in order to demonstrate the performance of the enhanced solid-shell element and assumed shell element in the limit case, which is not a matter of engineering practice but rather a subject of mathematical interest.

6. CONCLUSIONS

The solid-shell element, used for a SLF, is applied successfully to the FE-analysis of thin-walled structures. The three-dimensional material behaviour may be completely represented with non-degenerated constitutive models. The 7-parameter theory provides the distribution of thickness stress in contrast to the 5-parameter theory and performs as well as the degenerated shell approach, expect for the case of shells with unrealistic small thickness to length ratios. The MLF is able to approximate the exact results for the transverse stress fields arbitrarily closely. The resolution with the MLF of the transverse stress in the shell body under normal surface loading approximates the exact solution as a constant distribution in each layer. The EAS method, applied along with the MLF, improves the approximate results on coarse meshes in thickness direction.

DOI: 10.1002/cnm

REFERENCES

1. Schoop H. Oberflächenorientierte Schalentheorien endlicher Verschiebungen. *Ingenieur-Archiv* 1986; **56**:427–437.
2. Parisch H. A continuum-based shell theory for non-linear applications. *International Journal for Numerical Methods in Engineering* 1995; **38**:1855–1883.
3. Krätzig WB, Jun D. Multi-layer multi-director concepts for D-adaptivity in shell theory. *Computers and Structures* 2002; **80**:719–734.
4. Bathe K-J, Dvorkin E. Short communication a four-node plate bending element based on Mindlin/Reissner plate theory and a mixed interpolation. *International Journal for Numerical Methods in Engineering* 1985; **21**:367–383.
5. Verhoeven H. Geometrisch und physikalisch nichtlineare finite Plattenelemente mit Berücksichtigung der Dickenverzerrung. *Dissertation*, Technische Universität Berlin, 1992.
6. Betsch P, Stein E. An assumed strain approach avoiding artificial thickness straining for a non-linear 4-node shell element. *Computer Methods in Applied Mechanics and Engineering* 1995; **11**:899–909.
7. Braun M, Bischoff M, Ramm E. Nonlinear shell formulations for complete three-dimensional constitutive laws including composites and laminates. *Computational Mechanics* 1994; **15**:1–18.
8. Simo JC, Armero F. Geometrically non-linear enhanced strain mixed methods and the method of incompatible modes. *International Journal for Numerical Methods in Engineering* 1992; **33**:1413–1449.
9. Büchter N, Ramm E, Roehl D. Three-dimensional extension of non-linear shell formulation based on the enhanced assumed strain concept. *International Journal for Numerical Methods in Engineering* 1994; **37**:2551–2568.
10. Klinkel S, Gruttmann F, Wagner W. A continuum based three-dimensional shell element for laminated structures. *Computers and Structures* 1999; **71**:43–62.
11. Ramm E, Matzenmiller A. Large deformation shell analyses based on the degeneration concept. In *Finite Element Methods for Plate and Shell Structures*, Hughes TJR, Hinton E (eds). 1986.
12. Stander N, Matzenmiller A, Ramm E. An assessment of assumed strain methods in finite rotation shell analysis. *Engineering Computations* 1989; **6**:58–66.
13. Hüttel C, Matzenmiller A. Consistent discretization of thickness strains in thin shells including 3D-material models. *Communications in Numerical Methods in Engineering* 1999; **15**:283–293.
14. Zienkiewicz OC, Taylor RL. *The Finite Element Method*, *Vol. I*: *Basic Formulation an Linear Problems* (4th edn). McGraw-Hill: New York, 1989.
15. MacNeal R, Harder R. A proposed standard set of problems to test finite element accuracy. *Finite Elements in Analysis and Design* 1985; 3–20.
16. Vu-Quoc L, Tan XG. Optimal solid shell for non-linear analyses of multilayer composites I. Statics. *Computer Methods in Applied Mechanics and Engineering* 2003; **192**:975–1016.
17. Simo JC, Kennedy JG. On a stress resultant geometrically exact shell model. Part 5, Nonlinear plasticity: formulation and integration algorithms. *Computer Methods in Applied Mechanics and Engineering* 1992; **96**: 133–171.
18. Grashof F. *Theorie der Elastizität und Festigkeit mit Bezug auf ihre Anwendung in der Technik* (2nd edn). 1878.
19. Timoshenko SP, Goodier JN. *Theory of Elasticity* (3rd edn). McGraw-Hill: New York, 1982.
20. Matzenmiller A. Ein rationales Lösungskonzept für geometrisch und physikalisch nichtlineare Strukturberechnungen. *Dissertation*, Universität Stuttgart, 1988.

DOI: 10.1002/cnm